Journal of Materials Chemistry C

RSC Publishing

PAPER

View Article Online
View Journal | View Issue

Cite this: J. Mater. Chem. C, 2013, 1, 2183

Fluorinated 9,9′-spirobifluorene derivatives as host materials for highly efficient blue organic light-emitting devices†

Zhanfeng Li,[ab] Bo Jiao,[a] Zhaoxin Wu,*[a] Peng Liu,[a] Lin Ma,[a] Xiaoli Lei,[a] Dongdong Wang,[a] Guijiang Zhou,*[c] Huaiming Hu[d] and Xun Hou[a]

Received 22nd October 2012
Accepted 25th January 2013

DOI: 10.1039/c3tc00466j

www.rsc.org/MaterialsC

A series of new fluorinated 9,9′-spirobifluorene derivatives (SFs) have been designed and synthesized for organic light-emitting devices (OLEDs). The spatial structure of 2,2′,7,7′-tetrakis(2,4-bifluorophenyl)spiro-9,9′-bifluorene was determined by X-ray diffraction analysis. With the different substitution patterns of electron-withdrawing groups, such as F and CF_3, the photophysical properties, energy levels and thermal stabilities of these SFs can be tuned, which is supported by density functional studies of their geometries and electronic structures. A non-doped deep blue OLED using 2,2′,7,7′-tetrakis(3-fluorophenyl)spiro-9,9′-bifluorene (Spiro-(3)-F) as the emitter shows excellent Commission Internationale de l'Éclairage (CIE) coordinates of (0.169, 0.122) with emission peaking at *ca.* 408 nm. Furthermore, these SFs serve as an excellent host material for the 4,4′-bis(9-ethyl-3-carbazovinylene)-1,1′-biphenyl dopant to form high-performance OLEDs with low turn-on voltages and high efficiencies, especially for Spiro-(3)-F as the fluorescent host with pure blue CIE coordinates of (0.149, 0.187), a low turn-on voltage of 3.4 V, high luminance of over 10 000 cd m^{-2}, a high current efficiency of 6.66 cd A^{-1}, and a high external quantum efficiency of 4.92%. The high efficiency is attributed to the high carrier mobility together with the low injection barriers for both the electron and the hole in the Spiro-(3)-F-based device.

1 Introduction

Organic light-emitting diodes (OLEDs) have attracted much scientific and commercial interest in recent years because of their potential application in full-color displays and lighting sources.[1–3] Many developments have been made in the primary red, green, and blue (RGB) emitters to realize commercial full-color displays. In particular, it is difficult to develop blue-emitting materials with high efficiency, color purity, and long operation times due to their intrinsically wide band gap. As a result, the electroluminescence (EL) performance of blue light-emitting devices is usually not as good as that of their green- and red-EL counterparts. Despite many relevant studies related to blue phosphorescent OLEDs (PhOLEDs), attainment of high efficiency and long lifetime blue phosphorescent devices is very difficult because their device fabrication is limited by the non-availability of suitable triplet host materials. Hence blue fluorescent emitters that display colour purity and good performance statistics is still of prime importance for application in full-color displays.[4–7] It is well known that a dopant/host doped emitter system can significantly avoid concentration quenching of fluorescence and improve device performance in terms of EL efficiency and emissive color, as well as operational lifetime.[8] Various host materials for blue emitting OLEDs have been reported to date, which include anthracene,[9–11] di(styryl)arylene,[12] dipyrenylbenzenes,[13] oligofluorenes,[14,15] tetra(phenyl) silyl,[16] and oligoquinoline derivatives.[17–19] However, novel blue host materials with good thermal and morphological stabilities to afford blue emitters with high efficiencies and color purity are still desirable.

Spiro compounds with inherent rigid structures have been attracting attention as organic functional materials because of their specific physical properties, such as high glass transition temperatures, good solubility and their amorphous nature, which make them very promising as an approach for opto-electric materials. The unwieldy structure of fluorescent emitters based on the spiro concept also very effectively suppresses excimer formation frequently observed in the solid state of many fluorescent dyes, and the emission properties are thereby

[a]Key Laboratory of Photonics Technology for Information School of Electronic and Information Engineering, Xi'an Jiaotong University, Xi'an 710049, People's Republic of China. E-mail: zhaoxinwu@mail.xjtu.edu.cn; Fax: +86 029-82664867

[b]College of Physics and Optoelectronics, Taiyuan University of Technology, Taiyuan 030024, People's Republic of China

[c]Department of Chemistry, School of Science, Xi'an Jiaotong University, Xi'an 710049, People's Republic of China. E-mail: zhougj@mail.xjtu.edu.cn

[d]Department of Chemistry, Shaanxi Key Laboratory of Physico-Inorganic Chemistry, Northwest University, Xi'an 710069, People's Republic of China

† Electronic supplementary information (ESI) available: Cyclic voltammograms, DSC scans and electroluminescent properties for target compounds. CCDC 903069. For ESI and crystallographic data in CIF or other electronic format see DOI: 10.1039/c3tc00466j

stabilized.[20,21] Particularly, spirobifluorene compounds have excellent thermal and chemical stabilities and high quantum efficiencies as well as nondispersive ambipolar carrier transporting properties.[22,23] Fluorination has been used in the past decade as a route to induce stability and electron transport or ambipolar transport in organics by lowering the energy levels (both the highest occupied molecular orbital (HOMO) and the lowest unoccupied molecular orbital (LUMO) energy levels) in small molecules or polymers, especially for OLEDs.[24–29] Moreover, the C–H···F interactions, similar to hydrogen bonds, play an important role in the solid state organization of fluorine compounds bearing both C–F and C–H bonds, forming a typical π-stack arrangement which enhances the charge carrier mobility.[27,28,30,31] Based on these, we reported the synthesis, characterization, and EL properties of new host materials with a 9,9′-spirobifluorene core and various fluorinated end-capping groups, demonstrating that Spiro-(3)-F serves as a new example of a highly efficient blue-light-emitting host for use in OLEDs.

2 Results and discussion

2.1 Synthesis, structural characterization and theoretical computation

A series of new fluorinated 9,9′-spirobifluorene derivatives (SFs) were readily obtained by one-step Suzuki coupling between brominated 9,9′-spirobifluorene (Spiro-4Br) and the respective fluorinated phenylboronic acid in the presence of a palladium catalyst with yields ranging from 82% to 96%. The chemical structures and the synthetic route used to synthesise the SFs in this study are shown in Scheme 1. Two kinds of substituents (*i.e.*, F and CF_3) were introduced onto the periphery of the phenyl substituents of the SFs. By changing the number and position of the substituents, we systematically synthesized seven compounds. After purification by column chromatography and recrystallization, these newly synthesized SFs were purified further by train sublimation at a reduced pressure below 10^{-3} Pa and fully characterized with ^{1}H NMR and elemental analysis. High-pressure liquid chromatography (HPLC) analysis was carried out to check the purity of the materials, which was at least above 99.5%. The molecular structure of 2,2′,7,7′-tetrakis(2,4-bifluorophenyl)spiro-9,9′-bifluorene (Spiro-(2,4)-F) was further confirmed by single crystal X-ray analysis (Fig. 1), and the crystallographic data and structure refinement parameters are summarized in the Experimental section. Spiro-(2,4)-F crystallizes in the monoclinic space group $P2_1/n$. The functionalized spiro-9,9′-bifluorene consists of two molecular π-systems with equal functions *via* a common sp^3-hybridized atom. The crystal structure of Spiro-(2,4)-F shows the perpendicular arrangement (88.2°) of the aryl chains, which leads to a high steric demand of the resulting rigid structure. Moreover, the dihedral angles between the 2,4-difluorophenyl rings and the adjacent phenyl rings of spiro-9,9′-bifluorene are between 45.4° and 47.2°. Weak F···H and F···F interactions exist between the two adjacent 2,4-difluorophenyl-functionalized spiro-9,9′-bifluorenes, indicated by the minimum distances of F···H and F···F, which are 2.50 and 2.91 Å, respectively. Adjacent phenyl units are also linked *via* pairs of the complex π···π interactions with a shortest distance of 3.36 Å between the 2,4-difluorophenyl units, and the F···π interactions between the peripheral F atoms on the 2,4-difluorophenyl of one molecule and the phenyl rings of the next with a shortest distance of 3.16 Å.

Quantum chemical calculations performed by the DFT/B3LYP/6-31G(d,p) level in the Gaussian 03 program revealed that all the molecules adopted a cross-shaped molecular structure (Fig. 2). Particularly, the peripheral substituted phenyl groups are twisted with respect to the adjacent phenyl group of the spiro-9,9′-bifluorene core by an angle of 36.3–60.7° because of steric repulsion between the substituted phenyl peri-H (F or CF_3) atoms and the hydrogen atoms of the phenyl ring attached to the spiro-9,9′-bifluorene unit. The dihedral angle for the CF_3-substituted counterpart (Spiro-(2)-CF_3) is the largest due to the strongest steric effect of the peripheral CF_3-substituted phenyl at the *ortho*-position on the phenyl of the spiro-9,9′-bifluorene core in Spiro-(2)-CF_3. In the case of Spiro-(2,4)-F, the dihedral angles of the π plane of the 2,4-difluorophenyl rings and the adjacent phenyl rings of spiro-9,9′-bifluorene are between 38.0° and 40.4°. These calculated structural parameters are in excellent agreement with the experimental values from the X-ray diffraction (XRD) data. Such structural characteristics can influence some of their electronic and physical properties such as the suppression of conjugation. The electron density in the HOMOs of the SFs is located predominantly on the two perpendicular spiro-9,9′-bifluorene moieties. In the LUMOs of Spiro-(3)-F and Spiro-(3,5)-CF_3, π-electrons locate only on one half of the molecule, while the other electrons delocalize over the molecules. The calculated HOMOs and LUMOs of all the SFs are listed in Table 1.

2.2 Thermal properties

The synthesized SFs have good film forming abilities, which enable the formation of smooth and flat thin films without any pin-holes by thermal evaporation processes. This may be a result of the unique molecular conformation of SFs, which are non-coplanar according to the molecular design (Fig. 2). As stated in the aforementioned geometries of SFs, spiro compounds are generally characterized by a high glass transition temperature (T_g) due to their bulky shape. The T_gs of compounds Spiro-(2)-F, Spiro-(3)-F, Spiro-(4)-F, Spiro-(2,4)-F,

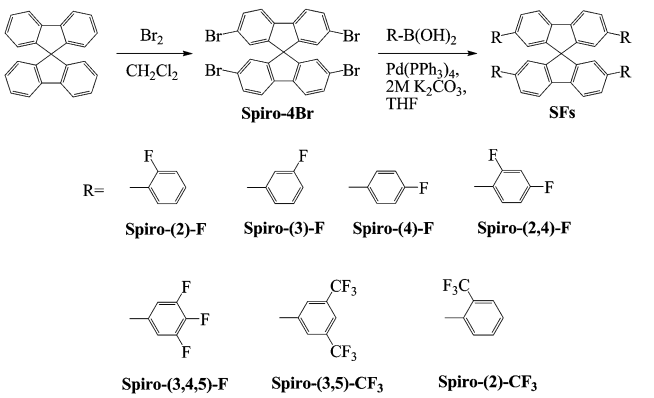

Scheme 1 Synthesis and structures of the SF compounds.

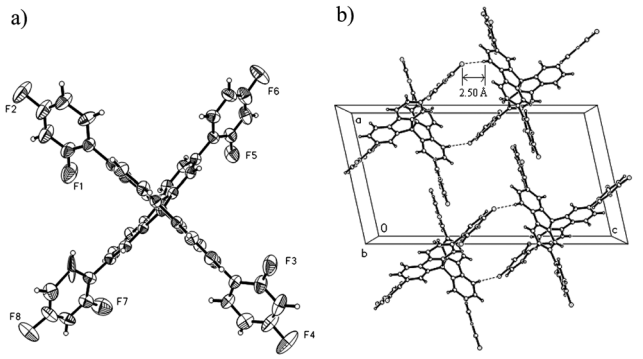

Fig. 1 (a) X-ray structure of Spiro-(2,4)-F with the thermal ellipsoids drawn at the 30% probability level. (b) Projection of the crystal structure of Spiro-(2,4)-F in the *ac* plane.

Spiro-(3,4,5)-F, and Spiro-(3,5)-CF_3 were determined to be 128, 119, 158, 90, 151, and 139 °C, respectively, by DSC in the second heating scans (for details, see ESI†), which are significantly higher than that of the most widely used host materials (*e.g.* 64 °C for DPVBi). In the DSC curves of Spiro-(2)-CF_3, no T_g was observed although the compound was heated to 320 °C. It is worth noting that, for Spiro-(2)-F, upon further heating beyond the T_g, an exothermal crystallization was observed at 183 °C (T_c), and a melting temperature (T_m) of 282 °C was detected. A clear T_m of Spiro-(2)-F was found to be 270 °C upon second heating. Their ability to form a thermally stable film by evaporation processes is highly desirable for application in OLEDs, since aggregation and microcrystallization generally have detrimental effects on the device stability.

2.3 Photophysical properties

Fig. 3 shows the optical absorption and photoluminescence (PL) spectra of SFs in CH_2Cl_2 dilute solutions and films (*ca.* 50 nm) obtained by thermal evaporation on a pre-cleaned quartz substrate. Their absorption behaviors differ significantly depending on the substitution of the spiro-9,9′-bifluorene moieties. The absorption features are similar for the F-substituted SFs (*i.e.* Spiro-(2)-F, Spiro-(3)-F, Spiro-(4)-F, Spiro-(2,4)-F and Spiro-(3,4,5)-F), which exhibit a common short-wavelength absorption band at *ca.* 310 nm and a long-wavelength band at *ca.* 330 nm. Likewise, Spiro-(2)-CF_3 and Spiro-(3,5)-CF_3 with CF_3 substitution exhibit similar features with absorption bands at *ca.* 290 and 320 nm. The UV-vis absorption of SFs shows the characteristic vibrational pattern of the isolated spiro groups both in the solid state and in solution. The similarities between the absorption spectra of dilute solutions and thin films suggests that the conformation of the solid state of SFs is similar to that of the solution state SFs, which is attributed to its non-coplanar structure to block aggregation effectively. The optical band gap values (E_g^{opt}, eV) for SFs were determined from their absorption onset potential edge of the absorption spectra in films. These values vary from 3.39 to 3.73 eV (Table 1).

As with the absorption spectra, the PL maximum varies depending on the number and position of the F or CF_3 substituents in SFs. The PL spectra of the *meta*-position fluorinated phenyl ring in the mono-substituted molecule Spiro-(3)-F appears to be significantly red-shifted with the most prominent peak appearing at 382 nm when compared with those of the *ortho*-position in Spiro-(2)-F (λ_{max} = 373 nm), the *para*-position in Spiro-(4)-F (λ_{max} = 378 nm), and the *ortho*- and *para*-positions in Spiro-(2,4)-F (λ_{max} = 371 nm). This is attributed to the double nature of the electronic effect of the fluorine atom, which is inductive and mesomeric. It is most electron-deficient in the *meta* position on the phenyl ring in Spiro-(3)-F because it is affected only by the inductive electron-withdrawing character of the fluorine atom. Contrary to this, in the case of Spiro-(2)-F, Spiro-(4)-F and Spiro-(2,4)-F, the coordinating carbon of the phenyl ring is less electron-deficient because the electron-withdrawing effect of the fluorine atom is compensated for by its electron-donating mesomeric character. As a consequence, the *meta* position on the phenyl ring in Spiro-(3)-F has better electron delocalization from the spiro-9,9′-bifluorene core to the peripheral substituted phenyl than the *ortho*- or/and *para*-positions in Spiro-(2)-F, Spiro-(4)-F and Spiro-(2,4)-F, and the emission level of Spiro-(3)-F is lower than that of Spiro-(2)-F, Spiro-(4)-F and Spiro-(2,4)-F. The emission maximum for Spiro-(3,4,5)-F in the solution state was observed at *ca.* 379 nm, which is located between Spiro-(3)-F and Spiro-(2)-F or Spiro-(4)-F. From the spectra in Fig. 1b, a blue shift can clearly be seen in the emission maximum for Spiro-(2)-CF_3 and Spiro-(3,5)-CF_3 relative to that for the F-substituted SFs by *ca.* 7–18 nm. When comparing the solution to the solid state, the emission maxima of the target compounds are only red-shifted 6–9 nm for the F-substituted SFs, due to the presence of weak interactions between the molecules (packing effect) in the solid state. The complex Spiro-(3,5)-CF_3 bearing CF_3 groups in the *meta*-positions with respect to the coordinating phenyl ring shows a red-shift in the emission by 19 nm in the films while that of the Spiro-(2)-CF_3 with a CF_3 group in the *ortho*-position appears to only be red-shifted by 1 nm, which is presumably due to varying degrees of planarization of the CF_3 substituted phenyl rings with respect to the central spiro-9,9′-bifluorene moieties within the amorphous phase (see Fig. 2). For all SFs, the difference in the dielectric constants in the two media, *i.e.*, solution and thin film, may additionally contribute to the observed red-shifted emissions upon going from solutions to films.[32,33] The absorption and PL spectra of these SFs were also studied in different organic solvents. Remarkably, both the absorption spectra and PL spectra of the SFs remain almost invariant when the solvent polarity is raised from 2.4 (toluene) to 5.8 (acetonitrile). This phenomenon was not believed to cause the unwanted EL red shift found in their doped devices.

We measured the fluorescence quantum yields (Φ_f) of the SPs in dilute CH_2Cl_2 solution using quinine sulfate as a standard (Φ_f = 0.56 in 1.0 M H_2SO_4 solution) at room temperature. All of the SFs exhibited high quantum yields in CH_2Cl_2 solution of between 0.92 and 0.98, which are comparable to that of their model compound 2,2′,4,4′-tetraphenyl-9,9′-spiro-bifluorene (Spiro-4Φ).[20] Their full width at half maximums (FWHMs) were in the range of 44–52 nm in films. The high quantum yield and narrow FWHM of each SF made it an excellent candidate for use as an efficient blue-light-emitting material in OLEDs.

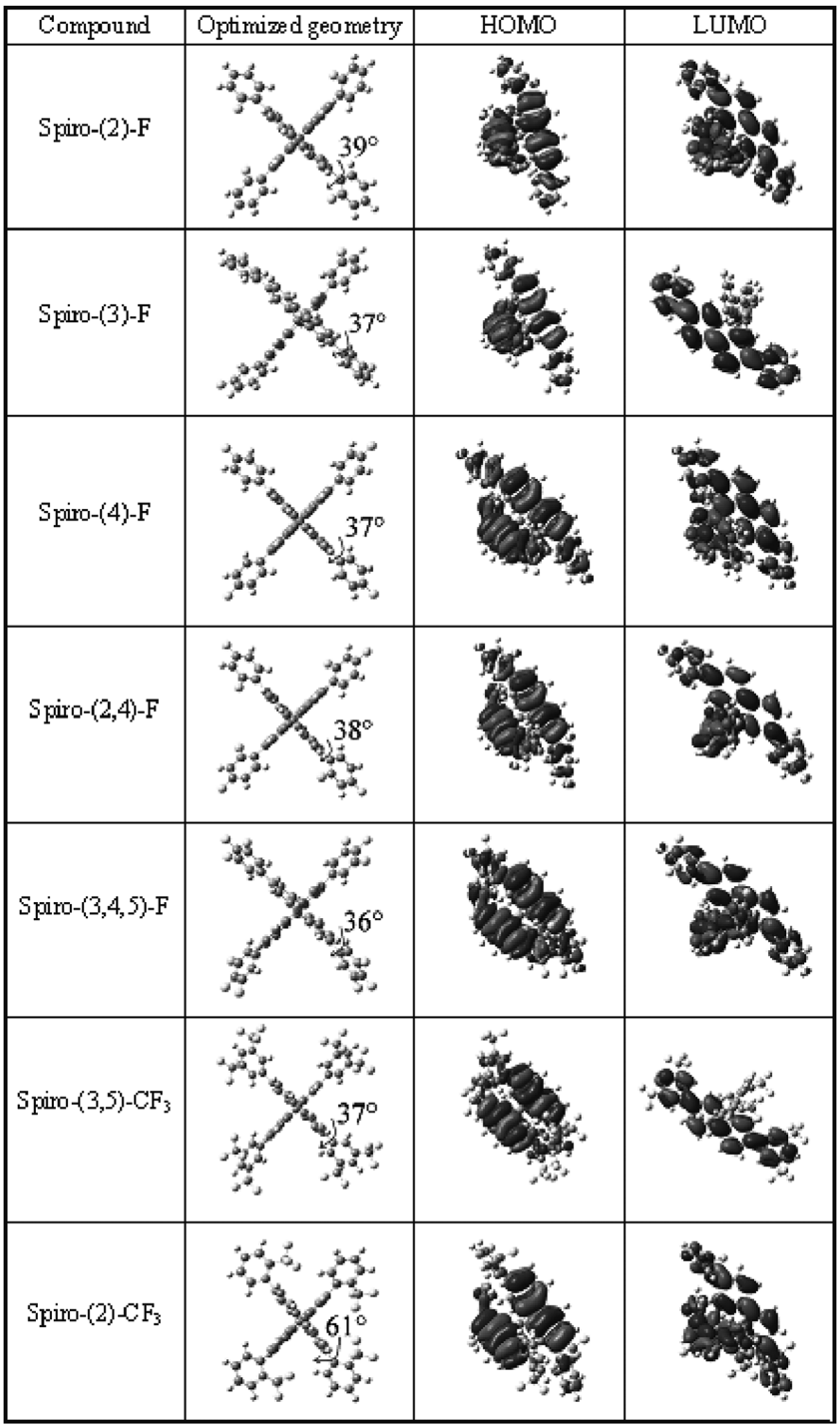

Fig. 2 The optimized geometries and the molecular orbital surfaces of the HOMOs and LUMOs for the SFs obtained at the B3LYP/6-31G level.

2.4 Electrochemical properties

Cyclic voltammetric (CV) studies were performed to calculate the HOMO and LUMO values for the SFs. The oxidation and reduction CV experiments were carried out in solutions of 0.1 M supporting electrolyte (n-Bu_4NPF_6) and 1 mM substrate in dry dichloromethane and acetonitrile, respectively, under a nitrogen atmosphere using ferrocene as an internal standard. The representative voltammograms for Spiro-(2)-F, Spiro-(3)-F, Spiro-(4)-F and Spiro-(2)-CF_3 are shown in Fig. 4 and all compounds exhibit an oxidation wave at potentials higher than that observed for ferrocene. The HOMO energy levels were estimated from the onset of oxidation potentials as summarized in Table 1. The values of the HOMOs for SFs thus calculated are between −5.80 and −6.14 eV and the relative HOMO level depends on the type of substituent and its position. Spiro-(3)-F with a mono-F substituent at the *meta*-position has a lower

Table 1 Physical properties of SFs

Compound	λ_{max}^{Abs} [ab] (nm)	λ_{max}^{PL} [ab] (nm)	Φ_f [c]	T_g/T_m [d] (°C)	E_{ox} [e] (V)	E_{red} [f] (V)	HOMO/LUMO^{exp} (E_g^{opt})[g] (eV)	HOMO/LUMO^{cal} ($\Delta E_{HOMO-LUMO}$)[h] (eV)
Spiro-(2)-F	306, 327/309, 329	359, 373/382	0.93	128/282	1.00	−1.12	−5.80/−2.29 (3.51)	−5.47/−1.38 (4.09)
Spiro-(3)-F	313, 333/313, 332	365, 382/371, 388	0.92	119/192	1.24	−1.06	−6.04/−2.65 (3.39)	−5.63/−1.54 (4.09)
Spiro-(4)-F	312, 333/313, 334	362, 378/369, 387	0.92	158/308	1.00	−1.07	−5.80/−2.35 (3.45)	−5.53/−1.42(4.11)
Spiro-(2,4)-F	305, 325/307, 330	355, 371/377	0.94	90/138	1.33	−0.90	−6.13/−2.62 (3.51)	−5.62/−1.52 (4.10)
Spiro-(3,4,5)-F	312, 333/313, 334	362, 379/370, 386	0.92	151/270	1.22	−1.09	−6.02/−2.61 (3.41)	−5.97/−1.89 (4.08)
Spiro-(3,5)-CF_3	287, 319/314, 329	366/370, 385	0.93	139/288	1.34	−1.06	−6.14/−2.73 (3.41)	−6.21/−2.13 (4.08)
Spiro-(2)-CF_3	291, 318/291, 381	364/365	0.98	na/310	1.01	−1.05	−5.81/−2.08 (3.73)	−5.69/−1.35 (4.34)

[a] Measured in CH_2Cl_2. [b] Measured in solid thin film on quartz plates. [c] Determined in CH_2Cl_2 using quinine sulfate ($\Phi_{PL} = 0.56$ in 1.0 M H_2SO_4 solution) as standard. [d] T_g: glass-transition temperature; T_m: melting point; na: not available. [e] Determined from the onset of oxidation potentials; measured in CH_2Cl_2; all of the potentials are reported relative to ferrocene, which was used as the internal standard in each experiment. The ferrocene oxidation potential was located at 0.13 V, relative to the Pt-wire reference electrode. [f] Determined from the onset of reduction potentials; measured in CH_3CN; all of the potentials are relative to ferrocene. The ferrocene oxidation potential was located at 0.19 V, relative to the Pt-wire reference electrode. [g] The HOMO and LUMO energies were determined from cyclic voltammetry and the absorption onset. $E_{HOMO} = -(qE_{ox} + 4.8)$ eV; $E_{LUMO} = E_{HOMO} + E_g^{opt}$. [h] Values from DFT calculation.

HOMO level (−6.04 eV) than that at the *ortho*- or *para*-positions (−5.80 eV). The HOMO energy level decreases with the number of F atoms. For example, the HOMO levels of Spiro-(2)-F and Spiro-(2,4)-F with mono- and di-F substituents determined from the electrochemical data are −6.13 and −5.80 eV, respectively. A similar situation was observed by Chen *et al.* for perylene bisimides and Gade *et al.* for 2,9-bisaryl-tetraazaperopyrene.[34,35] From the HOMO values and the optical band gap energies (E_g^{opt}) available from the UV-vis spectra (Table 1), the LUMO energies for the SFs were calculated to be in the range −2.08 eV to −2.73 eV. As expected, the Spiro-(2)-CF_3 had higher HOMO and LUMO values than Spiro-(3,5)-CF_3, since it has only one electron withdrawing CF_3 group, compared to two CF_3 groups in Spiro-(3,5)-CF_3. The electrochemical properties as well as the energy level parameters of the SFs are listed in Table 1. As shown in Table 1, the experimental HOMOs and LUMOs are in excellent agreement with the calculated values.

2.5 Carrier-transport properties

The carrier mobility of the Spiro-(3)-F thin film was characterized by the time-of-flight (TOF) transient-photocurrent technique.[36] The configuration of the device is ITO/Ag (60 nm)/Spiro-(3)-F (1.1 μm)/Ag (200 nm). The carrier mobility (μ) was calculated from the values of the transit time (T_t), the sample thickness (D) and the applied voltage (V) by using the following equation: $\mu =$

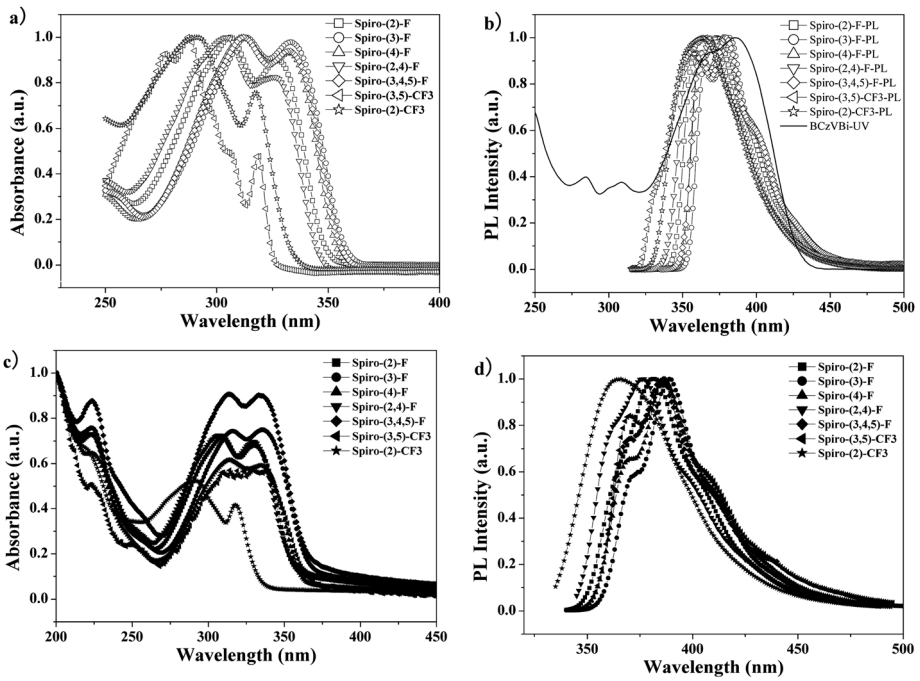

Fig. 3 (a) Absorption spectra of SFs in CH_2Cl_2. (b) PL spectra of SFs and absorption spectra of BCzVBi in CH_2Cl_2. (c) Absorption of SFs in thin films. (d) PL spectra of SFs in thin films.

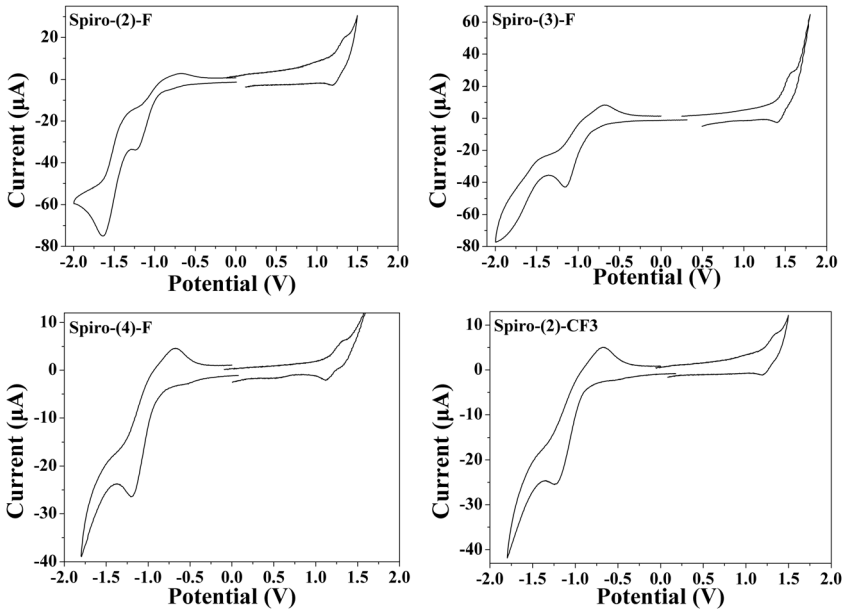

Fig. 4 Cyclic voltammograms of Spiro-(2)-F, Spiro-(3)-F, Spiro-(4)-F and Spiro-(2)-CF_3, in CH_2Cl_2 for oxidation and in CH_3CN for reduction.

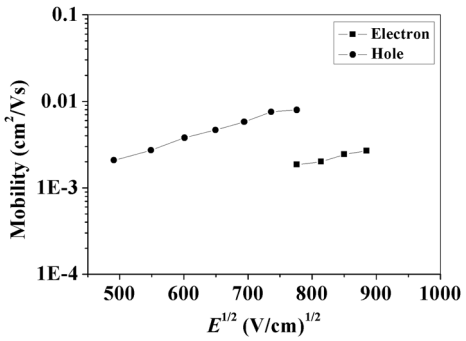

Fig. 5 Electron and hole mobilities *versus* $E^{1/2}$ for Spiro-(3)-F.

$D^2/(VT_t)$. As shown in Fig. 5, Spiro-(3)-F displays a high electron mobility ($\sim 10^{-3}$ cm^2 V^{-1} s^{-1}) at an electric field of 4×10^5 V cm^{-1}, which is comparable to the highest reported electron mobility,[37] and is about three orders of magnitude higher than that of the typical ETL material tris(8-hydroxyquinoline) aluminum (Alq_3), $\sim 10^{-6}$ cm^2 V^{-1} s^{-1} (at 0.8×10^6 V cm^{-1}).[38] Spiro-(3)-F also exhibits a high hole mobility that is close to the electron mobility. The mobility exceeds that of the typical hole transport material *N*,*N*′-bis(naphthalen-1-yl)-*N*,*N*′-bis(phenyl) benzidine (NPB) by more than one order of magnitude.[39]

2.6 Electroluminescent properties

In order to explore the OLED characteristics of SFs, we have fabricated non-doped blue devices, consisting of indium tin oxide (ITO)/molybdenum trioxide (MoO_3) (1 nm)/4,4′,4′-tris-(carbazol-9-yl)-triphenylamine (TcTa) (40 nm)/blue emitting layer (EML) (20 nm)/1,3,5-tris(1-phenyl-1*H*-benzimidazol-2-yl) benzene (TPBi) (40 nm)/LiF (1 nm)/Al (100 nm). MoO_3 was used as the hole injection layer (HIL), TcTa was used as the hole transporting layer (HTL), Spiro-(2)-F, Spiro-(3)-F, Spiro-(4)-F, Spiro-(2,4)-F, Spiro-(3,4,5)-F, Spiro-(3,5)-CF_3, and Spiro-(2)-CF_3 were used as the emitting layers (EML), TPBi was used as the electron transporting layer (ETL), and LiF was used as the electron injection layer (EIL), respectively. Fig. 6 shows the non-doped device structure and the energy levels of the materials used in the device fabrication. The non-doped deep blue OLED using Spiro-(3)-F as the emitter achieved excellent Commission Internationale de l'Éclairage (CIE) coordinates of (0.169, 0.122) with the emission peaking at *ca.* 408 nm, which are almost the

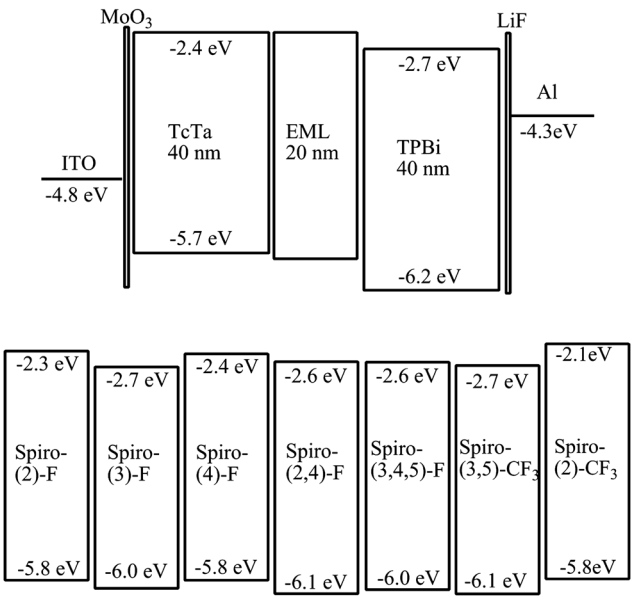

Fig. 6 Structures of the non-doped devices and the energy levels of the materials.

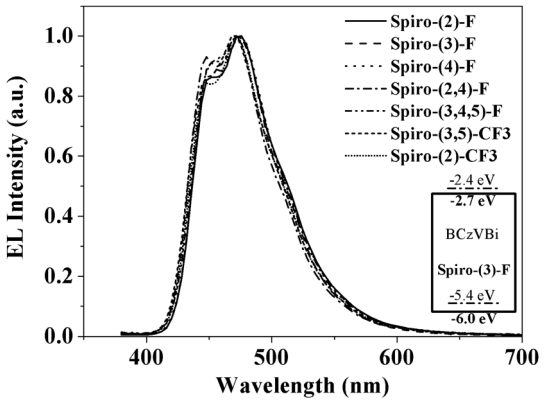

Fig. 7 EL spectra for OLEDs using 10 vol% BCzVBi doped in SF EMLs. Inset: energy band diagram of Spiro-(3)-F and BCzVBi.

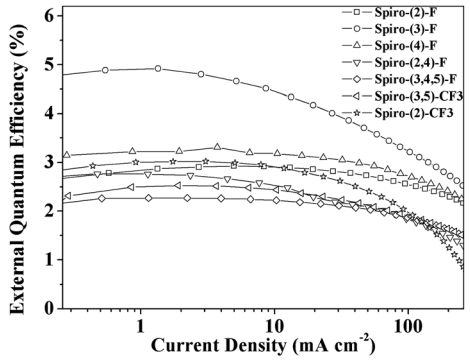

Fig. 9 External quantum efficiency (EQE) at different current densities for OLEDs using 10 vol% BCzVBi doped in SF EMLs.

same as those of its model compound (Spiro-4Φ) as a blue emitter (for details, see ESI†).[40]

To study the electroluminescence performance of SFs as blue host materials on the basis of SFs' wide band gaps, carrier transporting abilities, and film forming abilities, doping devices have been fabricated and evaluated by using the well known BCzVBi as the blue dopant. The device structures were the same as those of the non-doped devices, where each dopant was co-evaporated with the SFs to give 10 vol% dopant content (for details, see ESI†). Since the SF host materials have larger energy gaps of about 3.39–3.73 eV than the BCzVBi dopant ($E_g^{opt} \sim 3.00$ eV), and the spectral overlap efficiency between the PL spectra of SFs and the absorption spectra of the dopant is very high (Fig. 3b), Förster energy transfer was efficient from the SF hosts to the dopants. Fig. 7 shows the normalized EL spectra for the BCzVBi-doped SF devices. The CIE chromaticity coordinates of BCzVBi-doped SF devices are in the range (0.149–0.154, 0.169–0.192) at 10 V, which show pure blue emission characteristics with vibronic peaks around 448 and 472 nm.

Fig. 8 and 9 exhibit the current density–voltage–luminance–efficiency (J–V–L–η) characteristics of the BCzVBi-doped SF devices. The key device performance parameters and EL emission characteristics are summarized in Table 2. The BCzVBi-doped SF devices display low turn-on voltages (at which the luminance is 1 cd m^{-2}) no greater than 4.2 V. We also note that good to excellent performance of pure blue OLEDs can be achieved by using SFs as the hosts. The current efficiency and power efficiency of these devices are in the range 3.05–6.66 cd A^{-1} and 2.17–5.40 lm W^{-1}, respectively. The higher EL efficiencies of the BCzVBi-doped SFs can be attributed mainly to

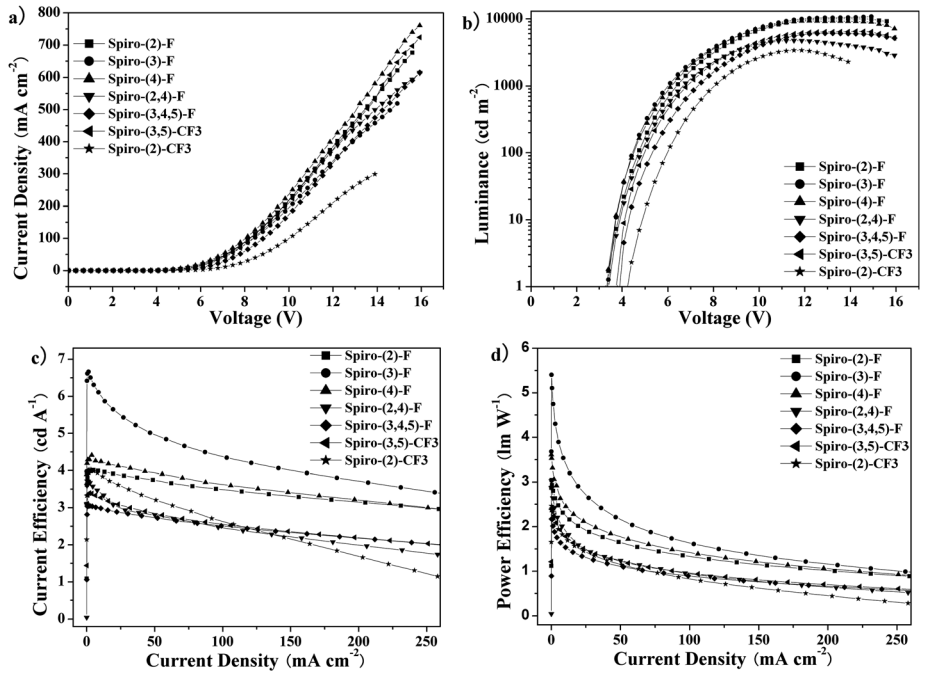

Fig. 8 (a) Current density–voltage curves, (b) brightness–voltage curves, (c) current efficiency–current density curves and (d) power efficiency–current density curves for OLEDs using 10 vol% BCzVBi doped in SF EMLs.

Table 2 EL performance of pure-blue devices with 10 vol% BCzVBi doped in EML

EML	λ_{max}^{EL} [a] (nm)	V_{on} [b] (V)	L_{max} [c] (cd m^{-2})	η_c [d] (cd A^{-1})	η_p [d] (lm W^{-1})	$\eta_{ext,\ max}$ [d] (%)	η_c [e] (cd A^{-1})	η_p [e] (lm W^{-1})	η_{ext} [e] (%)	CIE (x, y) [a]
Spiro-(2)-F:BCzVBi	448, 472	3.3	10 053	4.01	3.04	2.93	3.93	2.01	2.86	(0.153, 0.199)
Spiro-(3)-F:BCzVBi	450, 476	3.4	10 820	6.66	5.40	4.92	5.64	2.87	4.17	(0.149, 0.187)
Spiro-(4)-F:BCzVBi	449, 476	3.3	9310	4.41	3.61	3.31	4.16	2.20	3.10	(0.151, 0.192)
Spiro-(2,4)-F:BCzVBi	445, 472	3.4	4735	3.72	3.03	2.77	3.07	1.57	2.29	(0.152, 0.169)
Spiro-(3,4,5)-F:BCzVBi	448, 472	3.9	6083	3.05	2.17	2.27	2.91	1.37	2.15	(0.153, 0.189)
Spiro-(3,5)-CF_3:BCzVBi	448, 472	3.7	6501	3.40	2.40	2.53	3.14	1.57	2.32	(0.152, 0.178)
Spiro-(2)-CF_3:BCzVBi	448, 468	4.2	3381	4.03	2.47	3.02	3.66	1.51	2.72	(0.156, 0.183)

[a] Values collected at 10 V. [b] Turn-on voltage at 1 cd m^{-2}. [c] Maximum luminance. [d] Values collected at a peak efficiency. [e] Values collected at a current density of 20 mA cm^{-2}.

the efficient energy transfer from the SFs to the BCzVBi dopant. In addition, the hole trapping followed by the direct recombination with electrons at the dopant sites could additionally contribute to the enhanced EL efficiencies (see the energy band diagram of Spiro-(3)-F and BCzVBi in the inset of Fig. 7). The BCzVBi dopant can act as a hole trap for the BCzVBi-doped devices, because the HOMO level of BCzVBi is about −5.41 eV, which is higher than the host materials (from −5.80 to −6.14 eV). Notably, the device with Spiro-(3)-F as the host achieves the best EL performance, with a maximum luminance of over 10 000 cd m^{-2}, a maximum external quantum efficiency (EQE) as high as 4.92%, a maximum current efficiency of 6.66 cd A^{-1} and a maximum power efficiency of 5.40 lm W^{-1}. The performance of the Spiro-(3)-F device was outstanding compared to previously reported results for BCzVBi-doped fluorescence blue-light-emitting OLEDs.[17,41,42] For example, Kim *et al.* reported blue electroluminescence with a turn-on voltage of 10.7 V, a power efficiency of 1.27 lm W^{-1} and a maximum EQE of 3.83% from BCzVBi-doped fluorescent host molecules comprising covalently bonded carbazole and anthracene moieties;[41] and Lee *et al.* reported deep-blue electroluminescence with a power efficiency of 5.98 lm W^{-1} and a maximum EQE of 5.22% from a BCzVBi-doped phenylquinoline–carbazole derivative.[17]

The high efficiency of the Spiro-(3)-F-based device is attributed to a better balance of electron- and hole-transport properties (Fig. 5), which is due to the improved electron transport and injection. Since the LUMO levels of the Spiro-(3)-F host and TcTa are almost same, the barrier for electron injection from the TcTa layer to the emissive layer can be neglected. The barrier for hole injection from the HOMO of TcTa to the HOMO of Spiro-(3)-F is only 0.2 eV. Thus, the carrier charges will easily transport into the Spiro-(3)-F layer and recombine within this layer. As a result, a highly efficient, low-voltage OLED can be realized, because of the high carrier mobility together with the low injection barriers for both the electron and the hole in the Spiro-(3)-F-based device.

3 Conclusions

In summary, a series of efficient blue host materials of fluorinated 9,9′-spirobifluorene derivatives (SFs) have been successfully prepared by Suzuki coupling reactions in high yields. We have demonstrated that the absorption, emission, electrochemical properties, and OLED performances are significantly affected by the introduction of electron-withdrawing substituents such as F and CF_3 into the 9,9′-spirobifluorene core, which is supported by theoretical calculations employing the B3LYP functional. The non-doped deep blue OLED using Spiro-(3)-F as the emitter achieves excellent CIE coordinates of (0.169, 0.122) with the emission peaking at *ca.* 408 nm, which is almost the same as those with spiro-oligophenyl (Spiro-4Φ) as the blue emitter. Moreover, the use of Spiro-(3)-F as the host of the blue-emitting dopant BCzVBi resulted in a high-performance OLED with a high external quantum efficiency of 4.92%, a high current efficiency of 6.66 cd A^{-1} and a high power efficiency of 5.40 lm W^{-1} and pure blue emission with a maximum luminance of over 10 000 cd m^{-2}. The Spiro-(3)-F-based device exhibits an EQE close to almost 5%, which is one of the highest EQEs yet reported for BCzVBi-doped OLEDs to the best of our knowledge. These compounds are very efficient blue host materials because these have quite an effective spectral overlap with blue dopants such as BCzVBi.

4 Experimental

4.1 General information

Manipulations involving air-sensitive reagents were performed under an inert atmosphere of dry nitrogen. Commercially available reagents were used without further purification unless otherwise stated. 9,9′-Spirobifluorene, 2-fluorophenylboronic acid, 3-fluorophenylboronic acid, 4-fluorophenylboronic acid, 2,4-difluorophenylboronic acid, 3,4,5-trifluorophenylboronic acid, 3,5-bis(trifluoromethyl)phenylboronic acid, 2-(trifluoromethyl) phenylboronic acid and tetrakis(triphenylphosphine)palladium were purchased and used as received. 2,2′,7,7′-Tetrabromo-9,9′-spirobifluorene (Spiro-4Br) was prepared using the method reported and well characterized in the literature.[43] Absorption (UV) spectra were recorded on a Hitachi UV 3010 spectrophotometer. PL spectra were recorded on a Horiba Jobin Yvon Fluoromax-4 spectrophotometer. To measure the fluorescence quantum yields (Φ_f), degassed solutions of the compounds in CH_2Cl_2 were prepared. The concentration was adjusted so that the absorbance of the solution would be lower than 0.1. The excitation was performed at 334 nm, and quinine sulfate in 1.0 M H_2SO_4 solution, which has $\Phi_f = 0.56$, was used as a standard. Glass transition temperatures (T_g) were determined with a differential

scanning calorimeter (DSC, TA instruments DSC200PC) at a heating rate of 10 °C min^{-1} under a nitrogen atmosphere. Cyclic voltammetry (CV) was performed using a Princeton Applied Research model 273 A potentiostat at a scan rate of 100 mV s^{-1}. All experiments were carried out in a three electrode compartment cell with a Pt-sheet counter electrode, a glassy carbon working electrode and a Pt-wire reference electrode. Reduction CV was performed in acetonitrile and oxidation CV was performed in dichloromethane with 0.1 M of tetrabutylammonium hexafluorophosphate as a supporting electrolyte. The potential value was recorded relative to the oxidation potential of ferrocene, which was added to the electrolyte as an internal standard. The oxidation and reduction potentials were determined by taking the average of the anodic and cathodic peak potentials.

4.2 Single-crystal X-ray analysis

Diffraction data were collected at 293(2) K using graphite monochromated Mo Kα radiation ($\lambda = 0.71073$ Å) on a BRUKER SMART APEX II CCD diffractometer. The collected frames were processed with the software SAINT+ and an absorption correction (SADABS) was applied to the collected reflections. The structure was solved by direct methods (SHELXTL-97) and refined by the full-matrix-block least-squares method on F^2. Crystallographic data for Spiro-(2,4)-F: $C_{49}H_{24}F_8$, $M_r = 764.68$, crystal dimensions 0.30 × 0.18 × 0.12 mm^3, monoclinic, space group $P2_1/n$, $Z = 4$, $a = 13.8049$ (17) Å, $b = 12.2389$ (16), $c = 25.979$ (4), $\alpha = 90°$, $\beta = 102.745$ (3)°, $\gamma = 90°$, $U = 4281.2$ (10) $Å^3$, $\rho_{calcd} = 1.186$ g cm^{-3}, μ(Mo Kα) = 0.093 mm^{-1}, $F(000) = 1560$. A total of 21 161 reflections were measured in the range $2.93 \leq \theta \leq 25.05$ (*hkl* indices: $-13 \leq h \leq 16$, $-14 \leq k \leq 14$, $-30 \leq l \leq 30$), 7514 unique reflections. The structure was refined on F^2 to $R_1 = 0.1003$, $wR_2 = 0.3356$ (7514 reflections with $I > 2\sigma(I)$, GOF = 1.017 on F^2 for 523 refined parameters). CCDC number 903069.

4.3 Preparation of blue host SFs

THF (30 mL) and an aqueous solution of K_2CO_3 (2.0 M, 10 mL) were added to a flask containing 2,2′,7,7′-tetrabromo-9,9′-spirobifluorene (Spiro-4Br) (1.74 mmol), fluorinated phenylboronic acid (10 mmol) and $Pd(PPh_3)_4$ (0.35 mmol) under nitrogen. The reaction mixture was heated to reflux and maintained at this temperature for 24 h. When the reaction was completed (judging from thin-layer chromatography), water was added to quench the reaction. Then, the products were extracted with CH_2Cl_2. The organic portion was washed with brine, dried over anhydrous $MgSO_4$, and concentrated by evaporating off the solvent. The solid was absorbed on silica gel and purified by column chromatography using light petrol ether–ethyl acetate as the eluent to give the product.

4.3.1 2,2′,7,7′-Tetrakis(2-fluorophenyl)spiro-9,9′-bifluorene (Spiro-(2)-F). 1.05 g, white solid, yield: 87%. $T_m = 282$ °C. ^{1}H NMR ($CDCl_3$, 400 MHz): δ 6.98 (s, 4H), 7.01–7.10 (m, 8H), 7.18–7.23 (m, 4H), 7.28–7.31 (t, $J = 7.6$ Hz, 4H), 7.62 (d, $J = 7.6$ Hz, 4H), 7.93 (d, $J = 8.0$ Hz, 4H). Anal calcd for $C_{49}H_{28}F_4$: C, 84.96; H, 4.07. Found: C, 85.08; H, 4.02%.

4.3.2 2,2′,7,7′-tetrakis(3-fluorophenyl)spiro-9,9′-bifluorene (Spiro-(3)-F). 1.12 g, white solid, yield: 93%. $T_m = 192$ °C. ^{1}H NMR ($CDCl_3$, 400 MHz): δ 6.93–6.98 (t, $J = 7.2$ Hz, 4H), 7.01 (s, 4H), 7.16 (d, $J = 6.4$ Hz, 4H), 7.23–7.26 (t, $J = 7.6$ Hz, 4H), 7.28–7.31 (m, 4H), 7.67 (d, $J = 8.0$ Hz, 4H), 8.00 (d, $J = 8.0$ Hz, 4H). Anal calcd for $C_{49}H_{28}F_4$: C, 84.96; H, 4.07. Found: C, 84.85; H, 4.04%.

4.3.3 2,2′,7,7′-Tetrakis(4-fluorophenyl)spiro-9,9′-bifluorene (Spiro-(4)-F). 1.20 g, white solid, yield: 90%. $T_m = 308$ °C. ^{1}H NMR ($CDCl_3$, 400 MHz): δ 6.95 (s, 4H), 6.96–7.02 (t, $J = 8.8$ Hz, 8H), 7.38–7.41 (t, $J = 8.0$ Hz, 8H), 7.60 (d, $J = 8.0$ Hz, 4H), 7.95 (d, $J = 8.0$ Hz, 4H). Anal calcd for $C_{49}H_{28}F_4$: C, 84.96; H, 4.07. Found: C, 84.88; H, 4.09%.

4.3.4 2,2′,7,7′-Tetrakis(2,4-bifluorophenyl)spiro-9,9′-bifluorene (Spiro-(2,4)-F). 1.18 g, white solid, yield: 89%. $T_m = 138$ °C. ^{1}H NMR ($CDCl_3$, 400 MHz): δ 6.78–6.85 (m, 8H), 7.91 (s, 4H), 7.23–7.25 (m, 4H), 7.57 (d, $J = 8.0$ Hz, 4H), 7.93 (d, $J = 8.0$ Hz, 4H). Anal calcd for $C_{49}H_{24}F_8$: C, 76.96; H, 3.16. Found: C, 77.11; H, 3.12%.

4.3.5 2,2′,7,7′-Tetrakis(3,4,5-trifluorophenyl)spiro-9,9′-bifluorene (Spiro-(3,4,5)-F). 1.40 g, white solid, yield: 96%. $T_m = 270$ °C. ^{1}H NMR ($CDCl_3$, 400 MHz): δ 6.86 (s, 4H), 7.03–7.06 (t, $J = 7.6$ Hz, 8H), 7.560 (d, $J = 8.0$ Hz, 4H), 8.00 (d, $J = 8.0$ Hz, 4H). Anal calcd for $C_{49}H_{20}F_{12}$: C, 70.34; H, 2.41. Found: C, 70.40; H, 2.34%.

4.3.6 2,2′,7,7′-Tetrakis(3,5-bis(trifluoromethyl)phenyl)-spiro-9,9′-bifluorene (Spiro-(3,5)-CF3). 1.70 g, white solid, yield: 85%. $T_m = 288$ °C. ^{1}H NMR ($CDCl_3$, 400 MHz): δ 6.99 (s, 4H), 7.75–7.78 (m, 8H), 7.88 (s, 8H), 8.13 (d, $J = 8.0$ Hz, 4H). Anal calcd for $C_{57}H_{24}F_{24}$: C, 58.78; H, 2.08. Found: C, 58.86; H, 2.04%.

4.3.7 2,2′,7,7′-Tetrakis(2-(trifluoromethyl)phenyl)spiro-9,9′-bifluorene (Spiro-(2)-CF3). 1.10 g, white solid, yield: 82%. $T_m = 310$ °C. ^{1}H NMR ($CDCl_3$, 400 MHz): δ 6.98 (s, 4H), 7.02–7.10 (m, 8H), 7.21 (d, $J = 7.2$ Hz, 4H), 7.28–7.30 (t, $J = 8.0$ Hz, 4H), 7.63 (d, $J = 8.0$ Hz, 4H), 7.93 (d, $J = 8.0$ Hz, 4H). Anal calcd for $C_{53}H_{28}F_{12}$: C, 71.30; H, 3.16. Found: C, 71.21; H, 3.20%.

4.4 Device fabrication and testing

All of the organic materials were purified by temperature-gradient sublimation in a vacuum. The devices were fabricated by conventional vacuum deposition of the organic layers, LiF and an Al cathode onto an ITO-coated glass substrate under a base pressure lower than 1×10^{-3} Pa. The thickness of each layer was determined by a quartz thickness monitor. The voltage–current density (*V–J*) and voltage–brightness (*V–L*) as well as the current density–current efficiency (J–η_c) and current density–power efficiency (J–η_p) curve characteristics of the devices were measured with a Keithley 2602 and Source Meter. All measurements were carried out at room temperature under ambient conditions.

Acknowledgements

This work was financially supported by Basic Research Program of China (2013CB328701-2013CB328706), National Natural Science Foundation of China (Grant Nos. 61275034 and 61106123), Fundamental Research Funds for the Central Universities (Grant no. xjj2012087) and Natural Science Basic Research Plan in Shaanxi Province of China (no. 2012JQ8001).

References

1 C. W. Tang and S. A. VanSlyke, *Appl. Phys. Lett.*, 1987, **51**, 913.
2 L. S. Hung and C. H. Chen, *Mater. Sci. Eng., R*, 2002, **39**, 143.
3 S. R. Forrest, *Nature*, 2004, **428**, 911.
4 Y. Sun, N. C. Giebink, H. Kanno, B. Ma, M. E. Thompson and S. R. Forrest, *Nature*, 2006, **440**, 908.
5 G. Schwartz, S. Reineke, K. Walzer and K. Leo, *Appl. Phys. Lett.*, 2008, **92**, 053311.
6 G. Schwartz, T. H. Ke, C. C. Wu, K. Walzer and K. Leo, *Appl. Phys. Lett.*, 2008, **93**, 073304.
7 K. H. Lee, J. K. Park, J. H. Seo, S. W. Park, Y. S. Kim, Y. K. Kim and S. S. Yoon, *J. Mater. Chem.*, 2011, **21**, 13640.
8 C. W. Tang, S. A. VanSlyke and C. H. Chen, *J. Appl. Phys.*, 1989, **65**, 3610.
9 Y. H. Kim, D. C. Shin, S. H. Kim, C. H. Ko, H. S. Yu, Y. S. Chae and S. K. Kwon, *Adv. Mater.*, 2001, **13**, 1690.
10 J. Shi and C. W. Tang, *Appl. Phys. Lett.*, 2002, **80**, 3201.
11 Y. Kan, L. Wang, L. Duan, Y. Hu, G. Wu and Y. Qiu, *Appl. Phys. Lett.*, 2004, **84**, 1513.
12 C. Hosokawa, H. Higashi, H. Nakamura and T. Kusumoto, *Appl. Phys. Lett.*, 1995, **67**, 3853.
13 K. C. Wu, P. J. Ku, C. S. Lin, H. T. Shih, F. I. Wu, M. J. Huang, J. J. Lin, I. C. Chen and C. H. Cheng, *Adv. Funct. Mater.*, 2008, **18**, 67.
14 C. C. Wu, Y. T. Lin, K. T. Wong, R. T. Chen and Y. Y. Chien, *Adv. Mater.*, 2004, **16**, 61.
15 T. C. Chao, Y. T. Lin, C. Y. Yang, T. S. Hung, H. C. Chou, C. C. Wu and K. T. Wong, *Adv. Mater.*, 2005, **17**, 992.
16 L. H. Chan, H. C. Yeh and C. T. Chen, *Adv. Mater.*, 2001, **13**, 1637.
17 S. J. Lee, J. S. Park, K. J. Yoon, Y. I. Kim, S. H. Jin, S. K. Kang, Y. S. Gal, S. Kang, J. Y. Lee and J. W. Kang, *Adv. Funct. Mater.*, 2008, **18**, 3922.
18 C. J. Tonzola, A. P. Kulkarni, A. P. Gifford, W. Kaminsky and S. A. Jenekhe, *Adv. Funct. Mater.*, 2007, **17**, 863.
19 A. P. Kulkarni, A. P. Gifford, C. J. Tonzola and S. A. Jenekhe, *Appl. Phys. Lett.*, 2005, **86**, 061106.
20 T. P. I. Saragi, T. Spehr, A. Siebert, T. Fuhrmann-Lieker and J. Salbeck, *Chem. Rev.*, 2007, **107**, 1011.
21 R. Pudzich, T. Fuhrmann-Lieker and J. Salbeck, *Adv. Polym. Sci.*, 2006, **199**, 83.
22 C. Wu, T. L. Liu, W. Y. Hung, Y. T. Lin, K. T. Wong, R. T. Chen, Y. M. Chen and Y. Y. Chien, *J. Am. Chem. Soc.*, 2003, **125**, 3710.
23 Y. L. Liao, C. Y. Lin, Y. H. Liu, K. T. Wong, W. Y. Hung and W. J. Chen, *Chem. Commun.*, 2007, 1831.
24 J. Cornil, N. E. Gruhn, D. A. Dos Santos, M. Malagoli, P. A. Lee, S. Barlow, S. Thayumanavan, S. R. Marder, N. R. Armstrong and J. L. Brédas, *J. Phys. Chem. A*, 2001, **105**, 5206.
25 Z. Li, Z. Wu, B. Jiao, P. Liu, D. Wang and X. Hou, *Chem. Phys. Lett.*, 2012, **527**, 36.
26 J. S. Reddy, T. Kale, G. Balaji, A. Chandrasekaran and S. Thayumanavan, *J. Phys. Chem. Lett.*, 2011, **2**, 648.
27 M. L. Tang and Z. Bao, *Chem. Mater.*, 2011, **23**, 446.
28 F. Babudri, G. M. Farinola, F. Naso and R. Ragni, *Chem. Commun.*, 2007, 1003.
29 Z. Li, Z. Wu, W. Fu, P. Liu, B. Jiao, D. Wang, G. Zhou and X. Hou, *J. Phys. Chem. C*, 2012, **116**, 20504.
30 K. Reichenbächer, H. I. Süss and J. Hulliger, *Chem. Soc. Rev.*, 2005, **34**, 22.
31 R. Berger, G. Resnati, P. Metrangolo, E. Weber and J. Hulliger, *Chem. Soc. Rev.*, 2011, **40**, 3496.
32 J. Salbeck, N. Yu, J. Bauer, F. Weissörtel and H. Bestgen, *Synth. Met.*, 1997, **91**, 209.
33 J. N. Moorthy, P. Venkatakrishnan, P. Natarajan, D. F. Huang and T. J. Chow, *J. Am. Chem. Soc.*, 2008, **130**, 17320.
34 H. Z. Chen, M. M. Ling, X. Mo, M. M. Shi, M. Wang and Z. Bao, *Chem. Mater.*, 2007, **19**, 816.
35 S. C. Martens, T. Riehm, S. Geib, H. Wadepohl and L. H. Gade, *J. Org. Chem.*, 2011, **76**, 609.
36 M. F. Wu, S. J. Yeh, C. T. Chen, H. Murayama, T. Tsuboi, W. S. Li, I. Chao, S. W. Liu and J.-K. Wang, *Adv. Funct. Mater.*, 2007, **17**, 1887.
37 S. J. Su, T. Chiba, T. Takeda and J. Kido, *Adv. Mater.*, 2008, **20**, 2125.
38 Y. Li, M. K. Fung, Z. Xie, S. T. Lee, L. S. Hung and J. Shi, *Adv. Mater.*, 2002, **14**, 1317.
39 T. Y. Chu and O. K. Song, *Appl. Phys. Lett.*, 2007, **90**, 203512.
40 F. Steuber, J. Staudigel, M. Stössel, J. Simmerer, A. Winnacker, H. Spreitzer, F. Weissörtel and J. Salbeck, *Adv. Mater.*, 2000, **12**, 130.
41 S. H. Kim, I. Cho, M. K. Sim, S. Park and S. Y. Park, *J. Mater. Chem.*, 2011, **21**, 9139.
42 H. Park, J. Lee, I. Kang, H. Y. Chu, J. I. Lee, S. K. Kwon and Y. H. Kim, *J. Mater. Chem.*, 2012, **22**, 2695.
43 J. Pei, J. Ni, X. H. Zhou, X. Y. Cao and Y. H. Lai, *J. Org. Chem.*, 2002, **67**, 4924.

